

# Influence of runoff on coastal chlorophyll-a concentration in selected Philippine upwelling sites

Manuel Justin G. Custado\*<sup>1</sup> and Carlos Primo C. David<sup>2</sup>

<sup>1</sup>Institute of Environmental Science and Meteorology, University of the Philippines Diliman, Quezon City, 1101 Philippines

<sup>2</sup>National Institute of Geological Sciences, University of the Philippines Diliman, Quezon City, 1101 Philippines

## ABSTRACT

**T**his study assessed the relationship between runoff and chlorophyll-a in three documented upwelling sites in the Philippines. Linear correlation analysis between remotely sensed chlorophyll-a data and runoff from the Global Runoff Reconstruction (GRUN) dataset determined negative correlations along the coasts of Zamboanga del Norte and the Sulu Ridge and positive correlations off the coast of the Northern Bicol Shelf. The resulting correlations and generated temporal plots revealed the extent of the influence of runoff on productivity seasonally enhanced by upwelling. Generally, runoff had less effect on chlorophyll-a levels than the enhancement driven by upwelling during the northeast monsoon season. Upwelling was demonstrated to be a significant factor to productivity during months of lower runoff rates in Zamboanga del Norte and the Sulu Ridge. The dominance of weaker positive correlations ( $0.3 < |r| < 0.5$ ,  $p < 0.00001$ ) in the Northern Bicol Shelf suggests the limited influence of runoff on productivity despite the similarity in seasonal patterns within the area. The

trends and relationships determined in this study can be used in the management of coastal ecosystems and fisheries within the study sites, particularly in the context of future changes in the global climate.

## KEYWORDS

runoff, chlorophyll-a, GRUN, remote sensing, upwelling

## INTRODUCTION

The spatial and temporal patterns of productivity in coastal areas are highly variable due to the influence of terrestrial and oceanic processes that drive the distribution of nutrients. Terrestrial runoff can act as a medium of transport for nutrients and sediments supplied by a myriad of point and non-point sources (Beman, Arrigo, and Matson 2005, Jiang, Hao, and Fu 2016, Lihan et al. 2011). Several studies have demonstrated the positive correlation between runoff rates and phytoplankton levels in adjacent coastal waters (Beman, Arrigo, and Matson 2005, Lihan et al. 2011, Masotti et al. 2018, Wang et al. 2015). In other coastal sites, productivity is influenced by seasonal ocean dynamics that can generate upwelling. This is a process where cold, nutrient-rich water mass is driven to the surface, triggering the enhancement of productivity (Cabrera et al. 2011, Jing, Qi, and Du 2012, Villanoy et al. 2011).

\*Corresponding author

Email Address: [mgcustado@up.edu.ph](mailto:mgcustado@up.edu.ph)

Date received: December 01, 2020

Date revised: April 29, 2021

Date accepted: May 09, 2021

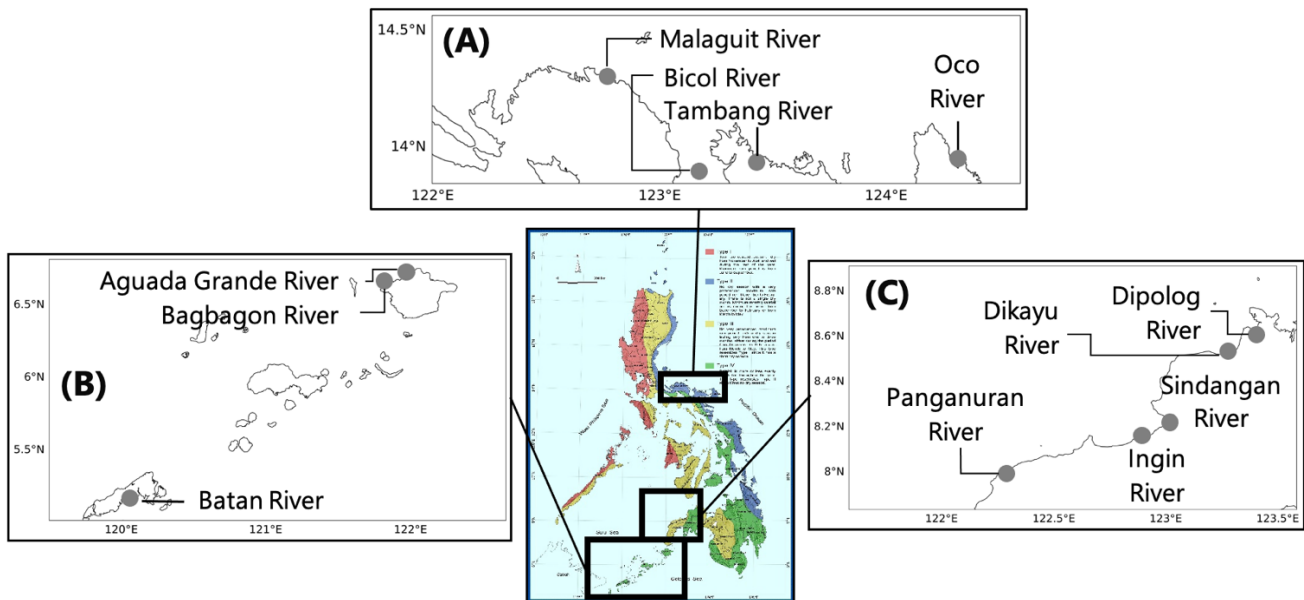


**Figure 1: The Philippine climate map (1951 - 2010) highlighting the study sites. Type I (Red), Type II (Blue), Type III (Yellow), Type IV (Green). Map illustrated by the Philippine Atmospheric Geophysical Astronomical Services Administration (2014). The featured coasts are (counterclockwise) (A) Northern Bicol Shelf, (B) Sulu Ridge, and (C) Zamboanga del Norte. Gray markers represent the locations of the outlet of some of the rivers draining to the coastal areas in each site.**

Monitoring the spatial and temporal variability of phytoplankton on the ocean surface has been accomplished by remote sensing techniques. Satellite-based sensors capture the spectral signature of chlorophyll-a, the pigment typically used as a biomass index for phytoplankton (Yap, Azanza, and Talaue-McManus 2004). The Sea-viewing Wide Field-of-view Sensor (SeaWiFS) and Moderate Resolution Imaging Spectroradiometer – Aqua (MODIS-Aqua) are among the several satellite-based sensors that can provide global chlorophyll-a datasets. SeaWiFS has provided data from September 1997 to December 2004, while MODIS-Aqua has generated data from July 2002 until the present. (Franz et al. 2005). Data from both sensors are regularly validated by the Ocean Biology Processing Group of NASA. The datasets produced over the years have been widely utilized in monitoring the spatiotemporal variability of chlorophyll-a in relation to runoff in sites such as the Gulf of California (Beman, Arrigo, and Matson 2005), Yangtze River Estuary (Wang et al. 2015), the coast of Tokachi Region in Japan (Lihan et al. 2011), and the coast of Central Chile (Masotti et al. 2018).

The Global Runoff Reconstruction (GRUN) is a dataset derived from a machine learning algorithm trained using global streamflow measurements. Published in 2019, the GRUN dataset provides a global database of monthly runoff from 1902 to 2014. The dataset, on average, was able to show better correspondence with available river discharge when validated against 13 global hydrological models (Ghiggi et al. 2019). Among the earliest local assessments of the GRUN dataset was with river gauging data in the Philippines, where the GRUN showed reasonable utility for spatiotemporal analysis (Ibarra et al. in press).

Climate in the Philippines is broadly classified into wet and dry seasons. Precipitation patterns are influenced by meteorological and topographical factors, particularly tropical cyclones and the Asian monsoons. The monsoons originate from the northeast (December to March) and southwest (June to October) (Wang, Wu, and Lau 2001). The resulting rainfall variability is used to group the country into four climate types, known as the modified Coronas classification (Coronas 1920). Type I identifies two distinct periods – dry from November to April and wet from May to October. Areas with Type II climate do not have a pronounced dry season, experiencing rain throughout the year that peaks

from December to February. Type III is similar to Type I but with a shortened dry season from November to April. Lastly, Type IV takes from Type II in having no marked dry season, with precipitation fairly distributed throughout the year.

A national scale analysis of the relationship of runoff and coastal chlorophyll-a was accomplished by Custado and David using the discussed datasets. They found a distinct distribution of positive and negative correlation coefficients across the country, with the former mostly located in open coasts while the latter found in internal seas (Custado and David in press). However, it is important to give context to these correlations, particularly in sites where extensive oceanographic processes that affect productivity take place.

Monsoonal winds blow through complicated bathymetry within the internal seas of the country, inducing stationary lee eddies and wind stress curl zones. This allows for the formation of potential upwelling sites (Chavanne et al. 2002; Pullen et al. 2008; Gordon and Ffield 2011). The coastal area of Zamboanga del Norte has been described in literature to experience upwelling as a result of these processes (Villanoy et al. 2011). On the other hand, persistent coastal upwelling observed in the Sulu Ridge has been attributed to internal tidal mixing, with monsoonal winds regulating the seasonal patterns of sea surface temperature (SST) and phytoplankton (Jing, Qi, and Du 2012). Potential upwelling sites in outer coastal areas have also been described in literature. Currents from the Pacific Ocean forced through the complex topography of the Northern Bicol Shelf were suggested to induce upwelling in its coastal waters (Amedo, Villanoy, and Udarbe-Walker 2002). Figure 1 illustrates the discussed potential upwelling sites, along with several of the river systems that drain into each study area.

Increases in phytoplankton levels linked to coastal upwelling are generally several magnitudes greater than the influence of riverine runoff. Hence, the process is usually assumed to support rich ecosystems and fisheries. However, published studies in the plume area of the Columbia River and the coastal area of Central Chile have implied that the inorganic nutrient fluxes coming from runoff were still essential to their respective coastal ecosystems despite experiencing seasonal upwelling (Hickey et al. 2010, Masotti et al. 2018). This contribution is particularly

important during phases of delayed upwelling or extended downwelling events (Hickey et al. 2010). The present paper aims to utilize the previously discussed datasets to determine linear correlations between the temporal patterns of runoff and chlorophyll-a in the featured sites and discuss how upwelling influence the resulting correlations. Assessments made can be utilized for the management of mariculture activities in these sites, particularly in the context of the changing climate.

## MATERIALS AND METHODS

### Data

Data used for this study were extracted from the monthly composites provided by the GRUN dataset and SeaWiFS and MODIS-Aqua data. The GRUN was retrieved from the ETH Zürich Research Collection data repository (<https://www.research-collection.ethz.ch/handle/20.500.11850/324386>). It provides 0.5° x 0.5° (approximately 55 km) runoff data from January 1902 to December 2014 (n = 1356). The spatial resolution of the dataset does not allow for a detailed discussion of the individual rivers in each site. Hence, a single data grid represents the runoff aggregate from the river systems that drain into the coastal area bounded by the grid.

The GRUN machine learning algorithm used data from the Global Streamflow Indices and Metadata Archive (GSIM) and the Global Runoff Data Centre (GRDC) Reference Dataset as training and validation data, respectively. Input data were screened according to a set of criteria which included data completeness and catchment size, resulting in the use of 7,627 GSIM and 214 GRDC stations (Ghiggi et al. 2019). Streamflow data from the Philippines were excluded from use due to the filtering measures implemented (Ibarra et al. in press). Runoff values were predicted by feeding the trained algorithm with temperature and precipitation data from the Global Soil Wetness Project Phase 3 (GSWP) (Ghiggi et al. 2019).

Monthly Level 3 chlorophyll-a standard mapped image (SMI) data from the sensors were retrieved from the National Aeronautics and Space Administration – Goddard Space Flight Center (NASA-GSFC) database (<https://oceancolor.gsfc.nasa.gov/l3/>). The acquired SeaWiFS and MODIS-Aqua data were of 9 km and 4 km spatial resolutions, respectively. The SeaWiFS data were from October 1997 to December 2010, while MODIS-Aqua data were from August 2002 to December 2019.

The ocean color reprocessing algorithms maintained by NASA were observed to overestimate chlorophyll-a concentrations within coastal regions due to the optical complexity of waters near shore (Gregg and Casey 2004; Lohrenz et al. 2008). The use of the data in this study is therefore limited only to the assessment of spatiotemporal variability and not to evaluate absolute values, for which remotely sensed datasets have been noted to be of adequate utility (Hopkins et al. 2013, Lohrenz et al. 2008, Masotti et al. 2018).

### Data pre-processing

The retrieved chlorophyll-a files were merged to produce a single time series dataset for each sensor. Along with the runoff data, these datasets were re-gridded to a common 9 km spatial resolution using the conservative nearest interpolation method. The pixels analyzed for each site were bounded by the following coordinates: 7.8° to 9.0°N and 121.7° to 123.5°E for the coastal waters of Zamboanga del Norte; 5.0° to 6.8°N and 119.5° to 122.7°E for coastal areas within the Sulu Ridge; and 13.8° to

14.6°N and 122.0° to 124.6°E for the Northern Bicol Shelf (Figure 1).

The runoff dataset was subjected to the bias correction procedure implemented by Ibarra et al. derived from their analysis of the log<sub>10</sub>-transformed GRUN dataset against data from 74 manually observed streamflow stations across the Philippines (Ibarra et al. in press). They noted an improvement in the nationwide root mean square (RMS) error parameter by an order of magnitude (from 2.348 to 0.292 mm/day) (Ibarra et al. in press). The correction is described by the equation below:

$$\log_{10} \text{ corrected GRUN} = (0.774)(\log_{10} \text{ predicted GRUN}) + 0.099 \quad (1)$$

A single time series dataset from the two chlorophyll-a datasets was produced for each site by applying Model II ordinary least squares (OLS) regression on each data pixel during the period of overlap, from August 2002 to September 2010 (Marrari, Piola, and Valla 2017). This step was implemented on log<sub>10</sub>-transformed data as the pigment biomass in marine waters is of natural log-normal distribution (Bricaud, Bosc, and Antoine 2002). Coefficients calculated from the regression were used to adjust the log<sub>10</sub>-transformed data from MODIS-Aqua, using SeaWiFS data as reference (Marrari, Piola, and Valla 2017).

The generated 22-year dataset consisted of SeaWiFS data from October 1997 to July 2002 and the adjusted MODIS-Aqua data from August 2002 to December 2019. The majority of the dataset came from the adjusted MODIS-Aqua to fill the several gaps found in the SeaWiFS dataset. Errors in the merged data were quantified by calculating the root mean square (RMS) and bias using the following equations:

$$\log \text{ RMS} = \sqrt{\frac{\sum [\log_{10}(\text{chl}_{\text{MODIS}}) - \log_{10}(\text{chl}_{\text{SeaWiFS}})]^2}{n}} \quad (2)$$

$$\log \text{ bias} = \sqrt{\frac{\sum [\log_{10}(\text{chl}_{\text{MODIS}}) - \log_{10}(\text{chl}_{\text{SeaWiFS}})]}{n}} \quad (3)$$

To address the problem of missing data due to cloud cover, the Data Interpolating Empirical Orthogonal Functions (DINEOF) method was adopted to fill in gaps in the merged chlorophyll-a dataset. The DINEOF is a self-consistent technique which iterates through a number of optimal Empirical Orthogonal Functions (EOFs) modes to return a complete matrix of data. The number of optimal iterations is determined by the last leading EOF mode which returns the smallest error (Beckers and Rixen 2003; Alvera-Azcárate et al. 2005). The DINEOF was originally used for sea surface temperature datasets (SST), but it was also employed to reconstruct chlorophyll-a datasets in several studies (Wang et al. 2015, Wang, Gao, and Liu 2019). Remote sensing data with more than 95% missing spatial and temporal values were excluded from the process.

The data pre-processing methodologies were carried out using Python programming language. Chlorophyll-a datasets were reconstructed using the Fortran-based DINEOF software developed by the GeoHydrodynamics and Environment Research (GHER) group, University of Liège (<http://modb.oce.ulg.ac.be/mediawiki/index.php/DINEOF>).

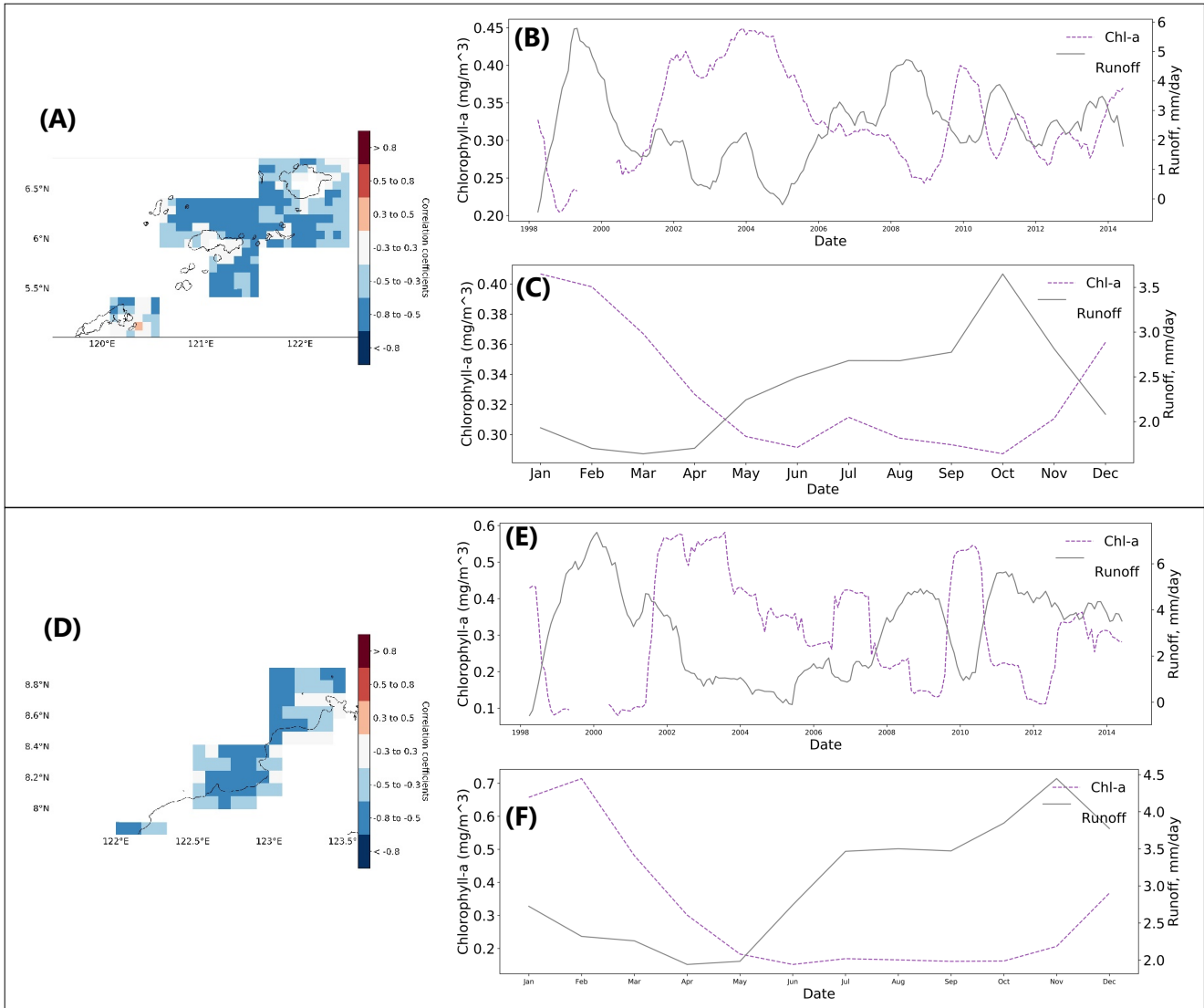


**Figure 2:** Correlations maps (A,D), and monthly (B,E) and seasonal (C,F) plots of chlorophyll-a (purple lines) and runoff (gray lines). Illustrated here are the negative correlations off the coasts of the Sulu Ridge (A)-(C) and Zamboanga del Norte (D)-(F). The monthly trends are deseasonalized and detrended.

### Data analysis

Trends in the data were derived using a sinusoidal equation with linear and seasonal components (Wang et al. 2015, Weatherhead et al. 1998). The model is defined by the following equation:

$$Y_t = \mu + \omega X_t + \beta \sin\left(2\frac{\pi}{j}X_t + \alpha\right) + N_t, \quad t = 1 \dots n \quad (4)$$

where  $Y_t$  is the mean monthly chlorophyll-a or runoff data;  $X_t$  is the time in months from the initial time point of the data;  $n$  is the length of the time series;  $\mu + \omega X_t$  is the linear trend component where  $\mu$  is a constant term and  $\omega$  is the variation trend; and  $\beta \sin\left(2\frac{\pi}{j}X_t + \alpha\right)$  is the seasonal component, where  $\beta$  is the amplitude of variation,  $j$  is the change cycle, and  $\alpha$  is the initial phase (Wang et al. 2015).  $N_t$  represents the residual error, the difference between the actual and fitted data (Wang et al. 2015, Weatherhead et al. 1998).

The significance of the trend was determined following the methods described by Weatherhead et al. (1998). Assuming that  $N_t$  is of a first-order autoregressive process with the following equation:

$$N_t = \Phi N_{t-1} + \varepsilon_t \quad (5)$$

where  $\Phi$  is the autocorrelation coefficient and  $\varepsilon_t$  is the autocorrelation noise. The precision of the calculated trend ( $\sigma_\omega$ ) is approximated by the autocorrelation coefficient ( $\Phi$ ), length of the time series ( $n$ ), and standard deviation of the residual errors ( $\sigma_N$ ) (Weatherhead et al. 1998). This is described by Equation 6, which is applied to the runoff dataset.

If the dataset has a level shift at a certain point in time due to a change in instrumentation, the component ( $\delta U$ ) is added to the sinusoidal model to account for the change (Equation 7). To calculate for the precision of the trend using this equation, the variable  $\tau$ , which represents the fraction of time before the intervention, is introduced. Equation 8 illustrates this modification (Weatherhead et al. 1998). This equation is applied to the merged chlorophyll-a dataset. Significance of the quantified trend ( $\omega$ ) at 95% confidence level is achieved when the condition  $\left|\frac{\omega}{\sigma_\omega}\right| > 2$  is satisfied.

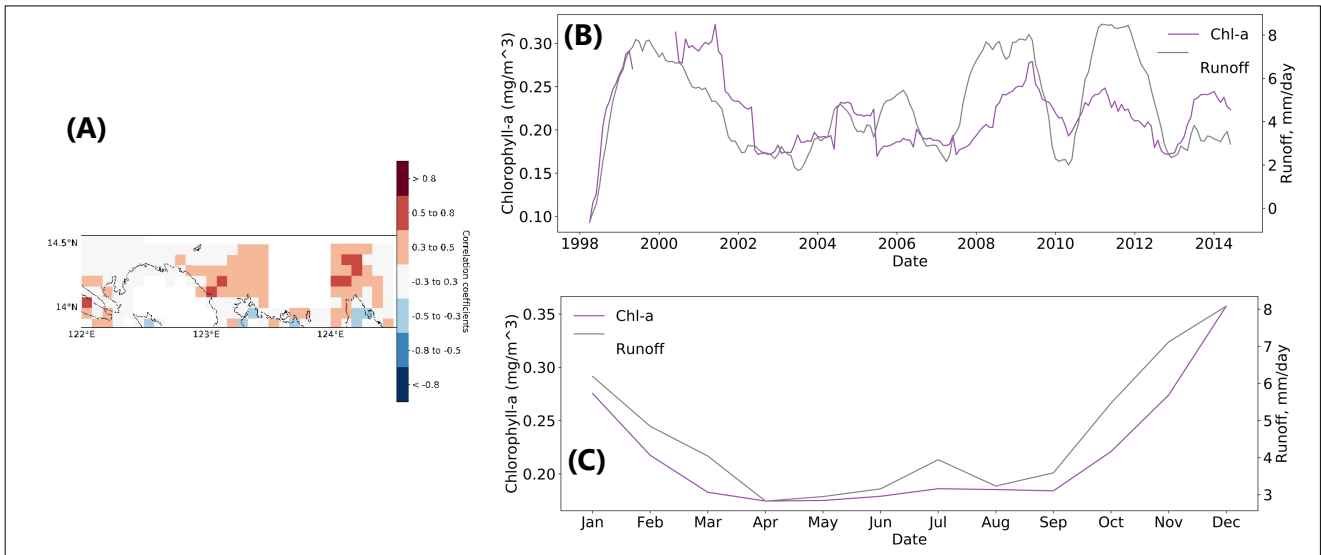


**Figure 3: Correlations maps (A), and monthly (B) and seasonal (C) plots of chlorophyll-a (purple lines) and runoff (gray lines) in the Northern Bicol Shelf. The monthly trends are deseasonalized and detrended.**

$$\sigma_{\omega} \approx \frac{\sigma_N}{n^{3/2}} \sqrt{\frac{1 + \Phi}{1 - \Phi}} \quad (6)$$

$$Y_t = \mu + \omega X_t + \beta \sin\left(2\frac{\pi}{j}X_t + \alpha\right) + \delta U + N_t, \quad t = 1 \dots n \quad (7)$$

$$\sigma_{\omega} \approx \left\{ \frac{\sigma_N}{n^{3/2}} \sqrt{\frac{1 + \Phi}{1 - \Phi}} \right\} \frac{1}{[1 - 3\tau(1 - \tau)]^{1/2}} \quad (8)$$

These equations were applied on the  $\log_{10}$ -transformed values of the adjusted and processed datasets. The calculations were carried out using Python.

Linear correlation analysis between each monthly pixel of the runoff and chlorophyll-a datasets was performed within the spatial and temporal overlaps of the data, which covered the period from October 1997 to December 2014 ( $n = 195$ ). The calculated correlation coefficients ( $r$ ) were evaluated and grouped according to the criteria defined by Huang (1990), which was adopted for use by Wang et al. in their analysis of the correlation between estuarine chlorophyll-a data and runoff from the Yangtze River (Wang et al. 2015). Correlation coefficients were grouped as follows:  $|r| < 0.3$  indicates no correlation,  $0.3 < |r| < 0.5$  indicates low correlation,  $0.5 < |r| < 0.8$ , indicates moderate correlation, and  $0.8 < |r| < 1.0$  indicates strong correlation (Huang 1990). This analysis, along with the generation of temporal plots were performed using the Python programming language.

## RESULTS

Figures 2 and 3 illustrate the correlations maps generated using the classifications set by Huang (1990), including the monthly and climatological seasonal plots from the three sites. The corresponding temporal plots were derived from the pixels classified with low and moderate correlations ( $0.3 < |r| < 0.8$ ), as no pixels were identified to be highly correlated. Summary of correlation coefficients calculated for each site are summarized in Table 1.

The linear trend parameters derived from the time series data are summarized in Table 2. The Sulu Ridge recorded small, but

statistically significant positive trends for both chlorophyll-a ( $\omega = 1.00 \times 10^{-4}$ ,  $\left|\frac{\omega}{\sigma_{\omega}}\right| > 2$ ) and runoff ( $\omega = 4.86 \times 10^{-5}$ ,  $\left|\frac{\omega}{\sigma_{\omega}}\right| > 2$ ). A slightly steep but statistically significant negative trend was also detected in the Northern Bicol Shelf ( $\omega = -3.913 \times 10^{-5}$ ,  $\left|\frac{\omega}{\sigma_{\omega}}\right| > 2$ ).

Negative correlation coefficients dominated the coasts of Zamboanga and Sulu Ridge. Accordingly, the observed runoff trends from these coasts exhibit inverse relationships with chlorophyll-a, as illustrated in the monthly and climatological seasonal plots generated. In both sites, chlorophyll-a reaches relatively higher levels during the months of December to February, peaking in January in the Sulu Ridge ( $0.407 \text{ mg/m}^3$ ) and February ( $0.739 \text{ mg/m}^3$ ) in Zamboanga. Chlorophyll-a minimums, on average, are experienced during the months of October ( $0.287 \text{ mg/m}^3$ ) in the Sulu Ridge and June ( $0.161 \text{ mg/m}^3$ ) in the coastal area of Zamboanga. The coastal areas in the Sulu Ridge receive the highest seasonal runoff rates during October ( $3.650 \text{ mm/day}$ ) and the lowest in March ( $1.639 \text{ mm/day}$ ). Meanwhile, the coastal waters of Zamboanga experience the highest seasonal runoff during November ( $4.431 \text{ mm/day}$ ), and the lowest in April ( $1.876 \text{ mm/day}$ ) (Figure 2c; f).

Positive correlations were also seen in the coastal areas within the Northern Bicol Shelf. However, the coverage of grids with low correlation appears to be more extensive than with moderate correlations. Chlorophyll-a and runoff highs and lows generally coincide during the same period; the highest levels are reached during December ( $0.357 \text{ mg/m}^3$  for chlorophyll-a and  $8.081 \text{ mm/day}$  for runoff) while the lowest are in September for chlorophyll-a ( $0.184 \text{ mg/m}^3$ ) and April for runoff ( $2.828 \text{ mm/day}$ ) (Figure 3c).

## DISCUSSION

Local and global scale climatic factors account for the seasonality evident from the generated time series plots. Strong upwelling events are often documented when the northeast monsoon (NEM) prevails in these sites. The stronger winds and cooler temperatures during the season allow for convective mixing (Udarbe-Walker and Villanoy 2001; Peñafior et al. 2007; Pullen et al. 2008; Villanoy et al. 2011), influencing the seasonality of the productivity in the study areas. This accounts for the enhanced chlorophyll-a concentration observed during

**Table 1: Calculated correlation coefficients (*r*) within the upwelling sites (*p*<0.00001).**

Site	Climate type	Total data count	No correlation				Low correlation				Medium correlation			
			<i>r</i> -values	Mean	Count	% of total count	<i>r</i> -values	Mean	Count	% of total count	<i>r</i> -values	Mean	Count	% of total count
Zamboanga del Norte	III	101	-0.295 - 0.089	-0.157	19	18.81	-0.499 - -0.302	-0.413	38	37.62	-0.677 - 0.549	-0.533	44	43.56
Sulu Ridge	IV	254	-0.296 - 0.233	-0.146	57	22.44	-0.499 - 0.404	-0.414	86	33.86	-0.736 - -0.503	-0.567	111	43.70
Northern Bicol Shelf	II	192	-0.192 - 0.298	0.132	113	58.85	-0.432 - 0.486	0.3	71	36.98	0.520 - 0.572	0.542	8	4.17

**Table 2: Linear trend parameters derived from the chlorophyll-a and runoff time series.**

	Chlorophyll-a (n = 266 months)			Runoff (n = 1356 months)		
	$\mu^*$	$\omega^*$	$\left  \frac{\omega}{\sigma_\omega} \right $	$\mu^*$	$\omega^*$	$\left  \frac{\omega}{\sigma_\omega} \right $
Zamboanga del Norte	-0.61	4.88 $\times 10^{-5}$	0.68	0.329	-4.83 $\times 10^{-6}$	1.02
Sulu Ridge	-0.59	1.00 $\times 10^{-4}$	5.80	0.19	4.86 $\times 10^{-5}$	10.12
Northern Bicol Shelf	-0.81	-3.91 $\times 10^{-5}$	2.04	0.57	3.21 $\times 10^{-6}$	0.85

the months of the NEM, especially seen in the temporal plots generated from the coastal areas of Zamboanga del Norte and the Sulu Ridge.

Runoff patterns differ across sites as each is governed by a different climate type. The illustrated seasonal trends off the coasts of Zamboanga del Norte and the Northern Bicol Shelf (Figure 2f, Figure 3c) are consistent with the rainfall patterns described by their respective climate types, Type III and Type II. In comparison, the seasonal runoff patterns in the Sulu Ridge, which falls under Type IV classification, exhibited a more variable pattern relative to the fairly even rainfall distribution described by its climate classification (Figure 2c). This is possibly due to other geographical factors that affect the hydrology of the area.

Apart from the local climate, global-scale processes such as the El Niño Southern Oscillations (ENSO) can influence runoff patterns. This phenomenon has been recorded to influence Philippine climate; its warm phase (El Niño) coincided with three of the four most significant drought events in the two decades before 2009, while its cold phase (La Niña) triggered flooding events more intense than normal (Hilarion et al. 2009, Corporal-Lodangco, Leslie, and Lamb 2016).

The influence of ENSO on runoff in the study sites can be demonstrated by cross correlating the generated monthly time series of runoff with the Multivariate ENSO Index (MEI) (Wolter and Timlin 1993). Negative correlations were calculated across all sites – highest coefficients were obtained at a time lag of 3 months in runoff within Zamboanga del Norte ( $r = -0.738$ ,  $p < 0.0001$ ,  $n = 778$ ), at a time lag of 2 months in the Sulu Ridge ( $r = -0.695$ ,  $p < 0.0001$ ,  $n = 778$ ), and at a time lag of 3 months in the Northern Bicol Shelf ( $r = -0.606$ ,  $p < 0.0001$ ,  $n = 778$ ). Positive MEI values correspond to the warm ENSO phase, while negative values correspond to the cold phase. Hence, the inverse relationships observed in each site suggest that the warm El Niño phase correspond to lower runoff rates and the cold La Niña phase trigger higher runoff rates.

Upwelling intensity in the three sites have also been described to be modulated by the ENSO phenomenon. Villanoy et al. (2011) and Jing et al. (2012) observed negative and positive correlations of SST with the ENSO index in Zamboanga del Norte and the Sulu Ridge, respectively. In the Northern Bicol Shelf, ENSO patterns shift the location of major oceanic currents that influence the area (Amedo, Villanoy, and Udarbe-Walker 2002), affecting the strength of upwelling that the area experiences.

#### Correlations off the coasts of Zamboanga del Norte and the Sulu Ridge

The enhancement of chlorophyll-a levels seen in these sites during the northeast monsoon coincides with declines in runoff rates, reflecting the negative correlation coefficients generated from the analysis. Upwelling enhances chlorophyll-a concentrations at a maximum of four times of the lowest chlorophyll-a mean in Zamboanga del Norte (max: 0.739 mg/m<sup>3</sup>; min: 0.161 mg/m<sup>3</sup>) and one and a half times of the lowest mean in the Sulu Ridge (max: 0.407 mg/m<sup>3</sup>; min: 0.287 mg/m<sup>3</sup>). The remarkable productivity enhancement in the waters off the coast of Zamboanga support a relatively significant sardine industry, as reported by Villanoy et al. in 2011 using sardine landing data and monthly chlorophyll-a values. Illustrating the relationship of runoff and chlorophyll-a in both sites are the mean composite images of the parameters during February and October, representing the NEM and SWM seasons (Figure 4 and Figure 5).

The accompanying SST images from the MODIS-Aqua satellite in Figures 4 and 5 further support the productivity enhancement illustrated by the chlorophyll-a data used. In particular, the uniformly cooler coastal waters of Zamboanga del Norte during the month of February (Figure 5c) demonstrate the monsoon-driven upwelling of colder, nutrient-rich waters that support the dramatic increase in chlorophyll-a concentration during the NEM season (Villanoy et al. 2011).

Masotti, et al. in 2018 described similar out of phase cycles between river discharge and chlorophyll-a in the coastal region of Central Chile. The chlorophyll-a concentration in identified

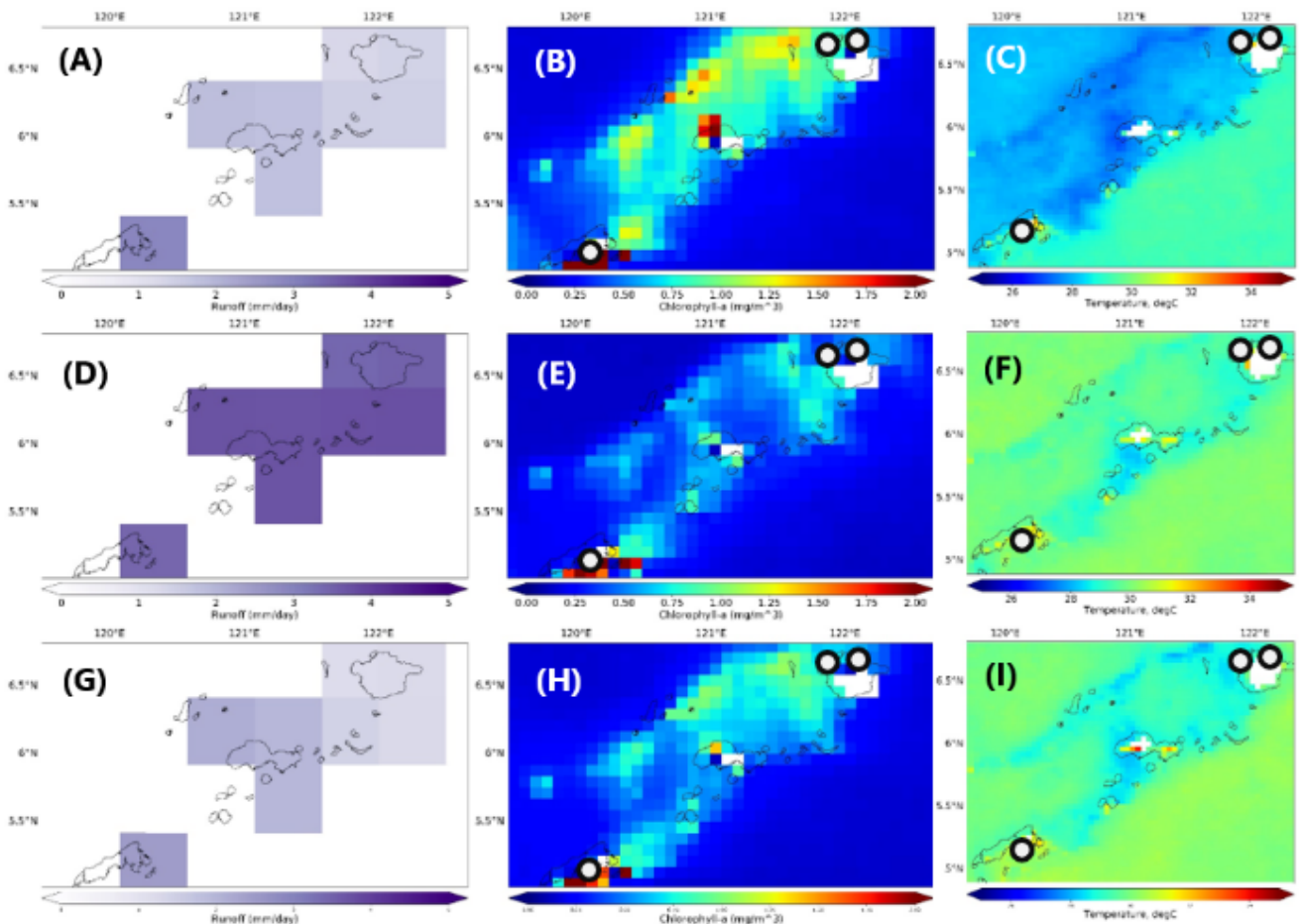


Figure 4: February (NEM), October (SWM), April (non-NEM/SWM) composites of runoff, chlorophyll-a, and SST in the Sulu Ridge. Upper panel: February runoff (A), chlorophyll-a (B), and SST (C); middle panel: October runoff (D), chlorophyll-a (E), and SST (F); lower panel: April runoff (G), chlorophyll-a (H), and SST (I). Warmer color corresponds to higher chlorophyll-a concentration and temperature. SST maps were derived from the MODIS-Aqua sensor. Circle markers correspond to the outlet of several of the river systems identified in the site (Refer to Figure 1B).

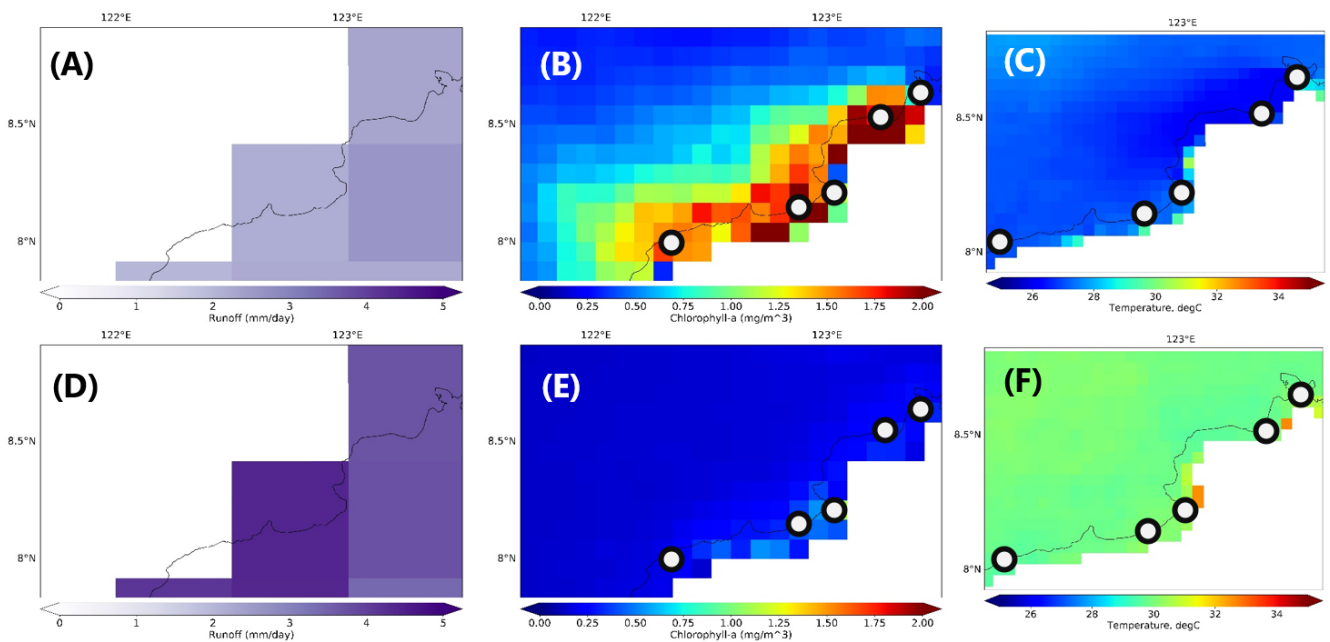
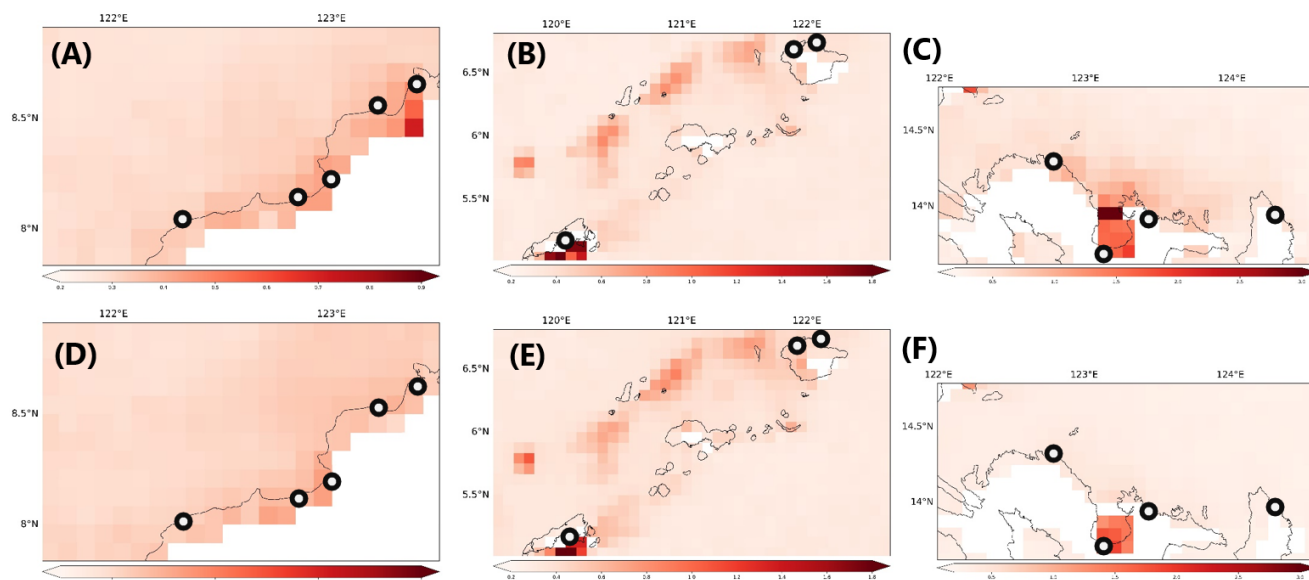


Figure 5: February (NEM) and January (SWM) composites of runoff, chlorophyll-a, and SST within the coast of Zamboanga del Norte. Upper panel: February runoff (A), chlorophyll-a (B), and SST (C); lower panel: October runoff (D), chlorophyll-a (E), and SST (F). Warmer color corresponds to higher chlorophyll-a concentration and temperature. SST maps were derived from the MODIS-Aqua sensor. Circle markers correspond to the outlet of several of the river systems identified in the site (Refer to Figure 1C).

river plume areas were magnitudes smaller when compared to the productivity enhancement experienced by the entire coastal region during seasonal upwelling events. Yet, researchers noted that this influence may still be adequate in sustaining local

ecosystem processes such as larval survival and recruitment, particularly during extended periods of downwelling or delayed upwelling (Hickey et al. 2010, Masotti et al. 2018).



**Figure 6: Radiance at 555 nm to illustrate river plume areas. Upper panel: during peak runoff months in Zamboanga del Norte (A, November), Sulu Ridge (B, October), and Northern Bicol Shelf (C, December); lower panel: during months of runoff lows in Zamboanga del Norte (D, April), Sulu Ridge (E, March), and Northern Bicol Shelf (F, April). Warmer color corresponds to stronger signal at the 555 nm band. Circle markers correspond to the outlet of several of the river systems identified in the site (Refer to Figure 1).**

A useful parameter to approximate the spatial extent of riverine influence is the normalized water-leaving radiance at the 555 nm band (nLw555). Several studies have used the reflectance at this wavelength to trace particulate matter and detect river plume signals associated with discharge (Masotti et al. 2018, Mazzini et al. 2015). Plots in Figure 6 illustrate the 9-km reflectance data at 555 nm acquired from SeaWiFS in the three study sites during months of highest and lowest mean runoff. However, the resolution of the data limits the identification of individual plumes from the rivers that drain into this site. Thus, the signals are interpreted as the aggregated influence of the rivers.

In Zamboanga del Norte, the month of November, when runoff is highest, records a slightly enhanced reflectance at 555 nm near the coast (Figure 6a) relative to April when runoff is lowest (Figure 6d). In contrast, the Northern Bicol Shelf sees a more significant enhancement of the signal in its coastal waters where the Bicol River Basin, a major catchment area, drains (Figure 6c, Figure 6f). Hence, the small magnitude of change in the reflectance at 555 nm nearshore of Zamboanga del Norte can be accounted for by the size of the adjacent river systems, which are smaller than the Bicol River Basin. This influence, albeit demonstrated as weak, may account for the chlorophyll-a levels during months when upwelling is absent.

In the Sulu Ridge, upwelling nearshore lasts throughout the year as consistent internal tidal mixing stimulate intense vertical velocity shear (Jing, Qi, and Du 2012). Depicted in the SST and chlorophyll-a images from October, a SWM month (Figure 4e-f) and April, a non-SWM/NEM month (Figure 4h-i) are cooler waters and high productivity within coastal areas despite the absence of the NEM. This enhancement reaches its maximum as monsoon-driven upwelling manifests in the northern side of the ridge. Chlorophyll-a and SST images for February show a distinct division of a cooler water mass northward accompanied by a phytoplankton bloom (Figure 4b-c). Continuous upwelling in the Sulu Ridge accounts for the weaker seasonal signal on coastal chlorophyll-a compared to Zamboanga del Norte.

Runoff influence in the Sulu Ridge appears to have minimal effect on productivity as persistent oceanographic processes dominate the area. Chlorophyll-a highs nearshore seem to not experience further enhancement despite higher runoff rates during the SWM season (Figure 4d-e) in comparison to the

lower runoff rates absent of monsoon influence (Figure 4g-h). In addition, there is no significant difference between the nLw555 plots of the site during March and October, when mean runoff rates are at its lowest and highest, respectively. However, the coarse resolution of the datasets is not sufficient to illustrate finer observations within the plumes generated by several minor rivers that run through the Sulu islands (Figure 1b).



**Figure 7: Bicol River Basin. Gray marker represents location of the Bicol River Basin outlet.**

#### Correlations within the coasts of the Northern Bicol Shelf

The Northern Bicol Shelf receives runoff from the Bicol River Basin, a major basin that drains into the San Miguel Bay (Figure 7). The spatial extent of its influence can particularly be observed during months of high runoff, as depicted by the expansion of the nLw555 signal outwards from San Miguel Bay during December (Figure 6c). Despite this, the calculated correlations in the Northern Bicol Shelf had larger coverage of  $r$  values categorized as low when compared to coefficients of moderate correlation (Figure 3a). Hence, the enhancement of chlorophyll-a levels during the NEM season can be more associated with upwelling than increased runoff. Limited runoff influence can also be seen during the month of July, where the small spike in mean rates did not appear to manifest greatly in the chlorophyll-a data during a similar period. The positive correlations observed can be attributed more to coinciding seasonal patterns rather than a relationship between the two

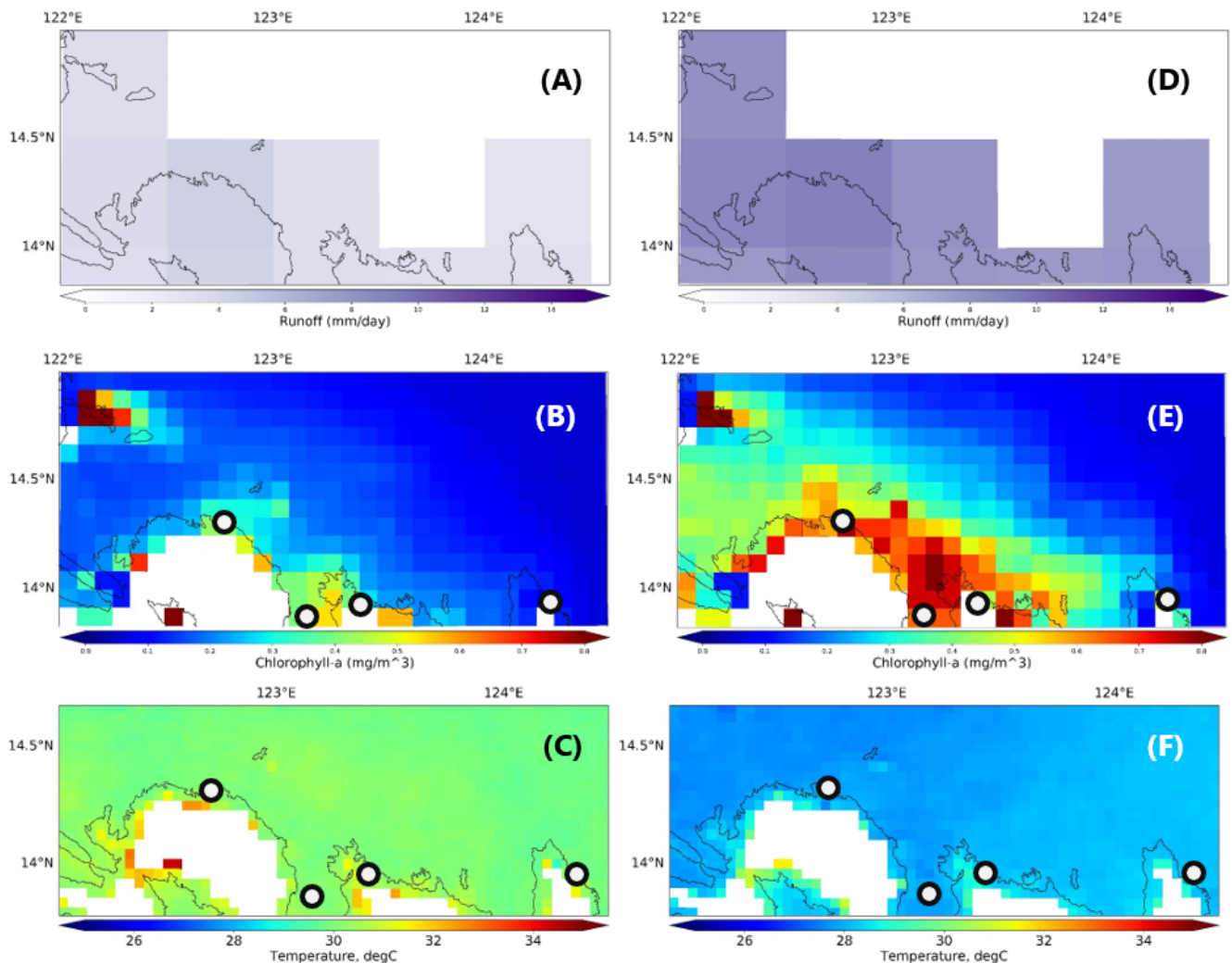


**Figure 8: December and September composites of climatological runoff, chlorophyll-a, and SST means within the coasts of the Northern Bicol Shelf. Left panel: September runoff (A), chlorophyll-a (B), and SST (C); right panel: December runoff (D), chlorophyll-a (E), and SST (F). Warmer color corresponds to higher chlorophyll-a concentration and temperature. SST maps were derived from the MODIS-Aqua sensor. Circle markers correspond to the outlet of several of the river systems identified in the site (Refer to Figure 1A).**

parameters (Figure 3c). Peak rainfall months in a Type II climate also occur during the NEM season.

Illustrating the observed patterns is Figure 8 which shows the composite runoff and chlorophyll-a images for December and September, representing the months with highest and lowest mean chlorophyll-a levels. There is a clear enhancement of productivity during the month of December, which extends even further from the shore. Upwelling in the Northern Bicol Shelf is suggested to be the result of the interaction of oceanographic processes driven by winds forced through the topography of the region (Amedo, Villanoy, and Udarbe-Walker 2002).

## CONCLUSIONS

This paper described the relationship between the temporal patterns of chlorophyll-a and runoff in selected upwelling sites in the Philippines using linear correlation analysis. Prevailing oceanographic processes in each site provided important context to the resulting correlations. The enhanced productivity levels in the Sulu Ridge and Zamboanga del Norte during the upwelling season resulted in an inverse relationship between runoff and chlorophyll-a. Runoff rates that peak during the SWM season in Zamboanga del Norte appeared to slightly enhance riverine influence based on the 555 nm reflectance data studied, possibly contributing to the chlorophyll-a levels during the absence of the

NEM. On the other hand, runoff had minimal effect on the productivity in the coastal areas of the Sulu Ridge due to the documented tidal actions that result in yearly persistent upwelling. The two parameters were found to follow similar seasonal patterns within the Northern Bicol Shelf, with the greater coverage of grids with weaker positive correlation coefficients suggesting that upwelling in this site contributes more to productivity than runoff.

The productivity patterns described in this study have significant consequences on coastal ecosystems and fishery activities. Local and global climatic factors influence the occurrence of upwelling and runoff. Therefore, fisheries in these sites, such as the sardine industry in the Zamboanga peninsula, can be left vulnerable to climate change. Integrating fisheries data with prevailing productivity patterns to determine their spatial and temporal correlations, as well as the collection of finer resolution datasets to further assess the influence of river plumes on productivity are recommended for future work.

## ACKNOWLEDGMENTS

The authors would like to acknowledge the following groups: National Aeronautics and Space Administration – Goddard Space Flight Center (NASA-GSFC) for the SeaWiFS and MODIS-Aqua data, the ETH Zürich Research Collection

database for the GRUN data and the GeoHydrodynamics and Environment Research (GHER) group of the University of Liège for the DINEOF software.

## CONFLICT OF INTEREST

The authors declare that there is no conflict of interest.

## CONTRIBUTIONS OF INDIVIDUAL AUTHORS

The writing and data manipulations were mostly done by the corresponding author. The second author was involved in the development of the general concept of the paper, providing significant inputs in the writing and analysis of data.

## REFERENCES

- Alvera-Azcárate A, Barth A, Rixen M, Beckers JM. Reconstruction of incomplete oceanographic data sets using empirical orthogonal functions: application to the Adriatic Sea surface temperature. *Ocean Model* 2005; 9(4):325–346.
- Amedo CL, Villanoy CL, Udarbe-Walker MJ. Indicators of upwelling at the northern Bicol Shelf. *UPV J Nat Sci* 2002; 7(1&2):42–52.
- Beckers JM and Rixen M. EOF calculations and data filling from incomplete oceanographic datasets. *J Atmos Ocean Technol* 2003; 20(12):1839–1856.
- Beman JM, Arrigo KR, Matson PA. Agricultural runoff fuels large phytoplankton blooms in vulnerable areas of the ocean. *Nature* 2005; 434(7030):211–214.
- Bricaud A, Bosc E, Antoine D (2002). Algal biomass and sea surface temperature in the Mediterranean Basin intercomparison of data from various satellite sensors, and implications for primary production estimates. *Remote Sens Environ* 2002; 81(2&3):163–178.
- Cabrera OC, Villanoy CL, David LT, Gordon AL. Barrier layer control of entrainment and upwelling in the Bohol Sea, Philippines. *Oceanography* 2011; 24(1):130–141.
- Chavanne C, Flament P, Lumpkin R, Dousset B, Bentamy A. Scatterometer observations of wind variations induced by oceanic islands: implications for wind-driven ocean circulation. *Can J Remote Sens* 2002; 28(3):466–474.
- Coronas J. *The Climate and Weather of the Philippines, 1903–1918*. Manila: Bureau of Printing, 1920:62–123.
- Corporal-Lodangco IL, Leslie LM, Lamb PJ. Impacts of ENSO on Philippine tropical cyclone activity. *J Climate* 2016; 29(5):1877–1897.
- Custado MJG and David CPC. Assessing the spatial and temporal relationship between coastal runoff and chlorophyll-a in the Philippines using gridded datasets. *J Coast Res* in press, 2021.
- Ghiggi G, Humphrey V, Seneviratne SI, Gudmundsson L. GRUN: An observations-based global gridded runoff dataset from 1902 to 2014. *Earth Syst Sci Data Discuss* 2019; (March):1–32.
- Gordon AL and Field A. Regional oceanography of the Philippine archipelago. *Oceanography* 2011; 24(1):14–27.
- Gregg WW and Casey NW. Global and regional evaluation of the SeaWiFS chlorophyll data set. *Remote Sens Environ* 2004; 93(4):463–479.
- Hickey BM, Kudela RM, Nash JD, Bruland KW, Peterson WT, Maccready P, Lessard EJ, Jay DA, Banas NS, Baptista AM, Dever EP, Kosro PM, Kilcher LK, Horner-Devine AR, Zaron ED, McCabe RM, Peterson JO, Orton PM, Pan J, Lohan MC. River influences on shelf ecosystems: Introduction and synthesis. *J Geophys Res Ocean* 2010; 115(2).
- Hilario F, de Guzman R, Ortega D, Hayman P, Alexander B. El Niño Southern Oscillation in the Philippines: Impacts, forecasts, and risk management. *Philippine Journal of Development* 2009; 36(1):9–34.
- Hopkins J, Lucas M, Dufau C, Sutton M, Stum J, Lauret O, Channelliere C. Detection and variability of the Congo River plume from satellite derived sea surface temperature, salinity, ocean colour and sea level. *Remote Sens Environ* 2013; 139:365–385.
- Huang HJ. *Investment Big Dictionary*. Beijing: Shanghai Social Science Press, 1990: 311–312.
- Ibarra D, David CP, Tolentino PL. Technical Note: Evaluation and bias correction of an observations-based global runoff dataset using historical streamflow observations from small tropical catchments in the Philippines. *Hydrol Earth Syst Sci Discuss* in press, 2020.
- Jiang D, Hao M, Fu J. Monitoring the Coastal Environment Using Remote Sensing and GIS Techniques. In: Marganky, M ed. *Applied Studies of Coastal and Marine Environments*. London: InTech, 2016:353–386.
- Jing Z, Qi Y, Du Y. Persistent upwelling and front over the Sulu Ridge and their variations. *J Geophys Res Ocean*, 2012; 117(11):1–18.
- Lihan T, Mustapha MA, Rahim SA, Saitoh S, Iida K. Influence of river plume on variability of chlorophyll a concentration using satellite images. *J Appl Sci* 2011; 11(3):484–493.
- Lohrenz SE, Redalje DG, Cai WJ, Acker J, Dagg M. A retrospective analysis of nutrients and phytoplankton productivity in the Mississippi River plume. *Cont Shelf Res* 2008; 28(12):1466–1475.
- Marrari M, Piola AR, Valla D. Variability and 20-year trends in satellite-derived surface chlorophyll concentrations in large marine ecosystems around south and western Central America. *Front Mar Sci* 2017; 4(372).
- Masotti I, Aparicio-Rizzo P, Yevenes MA, Garreaud R, Belmar L, Farías L. The influence of river discharge on nutrient export and phytoplankton biomass off the Central Chile coast (33°–37°S): seasonal cycle and interannual variability. *Front Mar Sci* 2018; 5(423).
- Mazzini PLF, Risien CM, Barth JA, Pierce SD, Erofeev A, Dever EP, Kosro PM, Levine MD, Shearman RK, Vardaro MF. Anomalous near-surface low-salinity pulses off the Central Oregon coast. *Sci Rep* 2015; 5(17145).

- Peñaflor EL, Villanoy CL, Liu CT, David LT. Detection of monsoonal phytoplankton blooms in Luzon Strait with MODIS data. *Remote Sens Environ* 2007; 109(4):443–450.
- Philippine Atmospheric Geophysical Astronomical Services Administration. Climate map of the Philippines (1951-2010). 2014.
- Pullen, J, Doyle, JD, May, P, Chavanne, C, Flament, P, Arnone, RA. Monsoon surges trigger oceanic eddy formation and propagation in the lee of the Philippine Islands. *Geophys Res Lett* 2008; 35(7):1–6.
- Udarbe-Walker MJB and Villanoy CL. Structure of potential upwelling areas in the Philippines. *Deep Res Part I Oceanogr Res Pap* 2001; 48(6):1499–1518.
- Villanoy, CL, Cabrera, OC, Yñiguez, A, Camoying, M, De Guzman, A, David, LT, Lament, PF. Monsoon-driven coastal upwelling off Zamboanga peninsula, Philippines. *Oceanography* 2011; 24(1):156–165.
- Wang B, Wu R, Lau KM. Interannual variability of the Asian summer monsoon: Contrasts between the Indian and the western north Pacific-East Asian monsoons. *J Clim* 2001; 14(20):4073–4090.
- Wang Y, Gao Z, Liu D. Multivariate DINEOF reconstruction for creating long-term cloud-free chlorophyll-a data records from SeaWiFS and MODIS: a case study in Bohai and Yellow Seas, China. *IEEE J Sel Top Appl Earth Obs Remote Sens* 2019; 12(5):1383–1395.
- Wang Y, Jiang H, Jin J, Zhang X, Lu X, Wang Y. (2015). Spatial-temporal variations of chlorophyll-a in the adjacent sea area of the Yangtze River estuary influenced by Yangtze River discharge. *Int J Environ Res Public Health* 2015; 12(5):5420–38.
- Weatherhead EC, Reinsel GC, Tiao GC, Meng XL, Choi D, Cheang WK, Keller T, DeLuisi J, Wuebbles DJ, Kerr JB, Miller AJ, Oltmans SJ, Frederick, JE. Factors affecting the detection of trends: Statistical considerations and applications to environmental data. *J Geophys Res* 1998; 103(D14):17,149–17,161.
- Wolter K and Timlin MS. Monitoring ENSO and COADS with a seasonally adjusted principal component index. *Proceedings of the 17<sup>th</sup> Climate Diagnostics Workshop* 1993;52-57.
- Yap LG, Azanza RV, Talaue-McManus L. The community composition and production of phytoplankton in fish pens of Cape Bolinao, Pangasinan: a field study. *Mar Pollut Bull* 2004; 49(9–10):819–832.